Development of a Kinetic Model of Hydrogen Absorption and Desorption in Magnesium and Analysis of the Rate-Determining Step

Yuta Kitagawa and Katsuaki Tanabe[*]

Department of Chemical Engineering, Graduate School of Engineering, Kyoto University,

Nishikyo-ku, Kyoto 615-8510, Japan

ABSTRACT

Mg is promising as a new light-weight and low-cost hydrogen-storage material. We construct a numerical model to represent the hydrogen dynamics on Mg, comprising dissociative adsorption, desorption, bulk diffusion, and chemical reaction. Our calculation shows a good agreement with experimental data for hydrogen absorption and desorption on Mg. Our model clarifies the evolution of the rate-determining processes as absorption and desorption proceed. Furthermore, we investigate the optimal condition and materials design for efficient hydrogen storage in Mg. By properly understanding the rate-determining processes using our model, one can determine the design principle for high-performance hydrogen-storage systems.

1. INTRODUCTION

Hydrogen storage in metals is an important technique for storing and transporting energy resources. Hydrogen-storage metals have high volumetric densities[1-3] because they store hydrogen in the solid state. However, they have poor gravimetric densities (because of their high weight) and are expensive (because of their low abundance). Recently, Mg-based materials have attracted a lot of attention as a light and cheap hydrogen-storage system[4,5] because Mg is a light-weight and earth-abundant material[6] and is able to store a large density of hydrogen, represented by a capacity of 7.6 wt%. However, the absorption and desorption kinetics of Mg are impractically slow and require high temperatures (above 600 K) for use[7].

The dynamics of hydrogen in metals consists of surface adsorption and desorption, surface-subsurface penetration, bulk diffusion, and hydride formation and decomposition reactions. There are three major reasons for the slow kinetics of hydrogen storage in Mg. First, the dissociative and recombinative activities of hydrogen molecules on the Mg surface are low; thus, the adsorption and desorption are slow. A large quantity of energy is required to dissociate hydrogen molecules on the Mg surface[8], while hydrogen molecules easily dissociate with low activation potential barriers on transition metals, such as Pd and Ni[9]. Second, diffusion of hydrogen in Mg, especially in MgH_2, is slow. The hydrogen diffusion rate in MgH_2 is several orders of magnitude lower than that in Mg, and subsequent hydrogen absorption is significantly hindered once a MgH_2 layer is generated on the surface[10,11]. Finally, MgH_2 is very stable, so it requires a very high temperature for decomposition; the decomposition reaction is slow, requiring a large amount of energy to extract hydrogen from Mg[12].

Much research has been conducted to improve the sorption kinetics in the Mg-hydrogen system[13]. For instance, ball milling[14,15], catalytic addition[15-17], and the use of composite materials with other

elements[18-20] are effective. Treatments that decrease the size of Mg[21,22] or enhance hydrogen dissociation and recombination are effective, and combinations of such effects to improve the hydrogen sorption rates are generally implemented[23,24]. Most of these treatments on Mg have been conducted in an empirical manner, and a few examples quantitatively investigated the dependence of hydrogen sorption rates on the process parameters and operation conditions. However, to efficiently design and optimize the structures and operation conditions of hydrogen-storage devices for practical use, a systematic understanding of the corresponding chemical reaction and transportation system by constructing an overall kinetic model is demanded in the community. In this study, we develop a kinetic model of hydrogen absorption and desorption on Mg toward a quantitative understanding of the hydrogen sorption mechanism.

Many models have been proposed for hydrogen-storage metals, and several have also been reported for Mg[25-27]. So far, most modeling of hydrogen-storage metals has assumed only a single rate-determining process; in reality, the rate-limiting step should vary based on the operation conditions and extent of sorption. The shrinking-core model[28,29], whereby the reaction occurs only at the surface of the core region, is commonly adopted to describe the chemical reaction; however, the reaction and diffusion occur simultaneously. Thus, we construct a model comprising multiple elementary processes to observe transitions of the rate-determining steps.

2. MODEL DEVELOPMENT

Dissolution of hydrogen into metals is generally expressed by the reaction in eq 1. A metal absorbs a stoichiometric amount (n mole per mole) of hydrogen and generates a hydride, MH_n:

$$M + \frac{n}{2}H_2 \underset{\leftarrow}{\overset{\rightarrow}{}} MH_n . \quad (1)$$

For Mg, $n = 2$, and MgH_2 is generated. The dynamics of hydrogen storage in Mg consists of: (i) dissociative adsorption and recombinative desorption at the surface, (ii) transportation between the surface and bulk regions, (iii) diffusion in the bulk, and (iv) hydriding and dehydriding reactions. The slow kinetics of hydrogen absorption and desorption in Mg stems from the low surface hydrogen activity, slow hydrogen diffusion in Mg (particularly in the hydride phase), and high stability of MgH_2. We develop a model that accounts for steps (i) and (iii), and the dehydriding reaction in step (iv) for the hydrogen desorption process. Figure 1 shows a schematic of the model, and Figure 2 shows a potential energy diagram of hydrogen in the gas phase and in Mg. We assume that the Mg particle is a sphere with radius R_0, and consider the hydrogen concentration distribution only in the radial direction. We neglect the volume change of Mg during hydrogen absorption and desorption for simplification as the first construction of an all-process-inclusive model (n.b., Our model still exhibits excellent reproduction of experimental results, as shown in the following.). We categorize the hydrogen states in the metal as one in which interlattice hydrogen exists as an atom and can freely diffuse, and another in which hydrogen is confined in the metal lattice. We define the hydrogen local concentration at the position of radius r in the Mg particle as $C_H(r)$ and $C_{MH}(r)$ for each of the states, respectively. The total hydrogen concentration, $C(r)$, is described as the sum of $C_H(r)$ and $C_{MH}(r)$, as shown in eq 2. This conceptual division of the concentrations of the hydrogen atom and the hydride provides convenient simplification and clarification in the formulation and computation as a development of practical model. Also experimentally, spatially

random, patchy distribution of the hydride regions are observed[30], and therefore the hydrogen and hydride regions may actually coexist at a radial position r, unlikely for the conventional, spherically symmetric shrinking-core model. The surface coverage fraction, θ, on the Mg particle surface is defined in eq 3, where n is the stoichiometric coefficient for hydrogen relative to the metal as appearing in eq. 1. We define the overall hydrogen content, X, in eq 4.

$$C(r) = C_{\mathrm{H}}(r) + C_{\mathrm{MH}}(r) \tag{2}$$

$$\theta = \frac{C(R_0)}{n} = \frac{C_{\mathrm{H}}(R_0)}{n} \tag{3}$$

$$X = \frac{3}{R_0^{\,3}} \int_0^{R_0} r^2 C(r) \mathrm{d}r \tag{4}$$

The dissociative-adsorption flux of the hydrogen atoms onto the metal surface is described as:

$$j_{\mathrm{ads}} = 2 s^0 \Gamma_{\mathrm{H_2}} \exp\left(-\frac{E_{\mathrm{ads}}}{RT}\right)(1-\theta)^2, \tag{5}$$

where s^0, E_{ads}, R, and T are the capturing coefficient, activation energy, gas constant, and absolute temperature, respectively[31]. The impingement rate of hydrogen molecules, $\Gamma_{\mathrm{H_2}}$, is described by eq 6 from the kinetic theory of gases:

$$\Gamma_{\mathrm{H_2}} = \frac{P_{\mathrm{H_2}}}{\sqrt{2\pi M_{\mathrm{H_2}} RT}}, \tag{6}$$

where $P_{\mathrm{H_2}}$ and $M_{\mathrm{H_2}}$ are the partial pressure and molar mass of hydrogen molecules, respectively. The recombinative-desorption rate is described as:

$$j_{\mathrm{des}} = k_{\mathrm{des}}^0 \exp\left(-\frac{E_{\mathrm{des}}}{RT}\right) N_{\mathrm{surf}} \theta^2, \tag{7}$$

where k_{des}^0, E_{des}, and N_{surf} are the frequency constant, activation energy, and number of surface sites[30]. The bulk-diffusion flux of hydrogen atoms in Mg is described as:

$$j_{\mathrm{dif}}(r) = -D_{\mathrm{H}} \frac{\partial C_{\mathrm{H}}}{\partial r}. \tag{8}$$

The diffusion coefficient, D_{H}, is dependent on the temperature and hydrogen concentration, as in eq 9. We determine β from the diffusion-coefficient data for Mg[32] and MgH_2[33]:

$$D_{\mathrm{H}} = D_{\mathrm{H}}^{0} \exp\left(-\frac{E_{\mathrm{dif}}}{RT}\right) \exp\left(-\beta \frac{C(r)}{n}\right). \tag{9}$$

Generally, the chemical reaction comprises the hydriding and dehydriding reactions; in this work, we only account for the MgH_2 decomposition reaction and neglect the hydriding reaction, which is sufficiently fast. The rate of the decomposition reaction in the absorption and desorption processes is expressed by:

$$u_{\mathrm{dec}} = \begin{cases} 0 & \text{(in absorption process)} \\ k_{\mathrm{dec}}^{0} \exp\left(-\dfrac{E_{\mathrm{dec}}}{RT}\right) C_{\mathrm{MH}}(r) & \text{(in desorption process)} \end{cases}, \tag{10}$$

where k_{dec}^{0} and E_{dec} are the frequency factor and activation energy, respectively. By using the calculated flux and reaction rate, the time evolution of θ, C_{H}, and C_{MH} are described as follows:

$$\frac{\mathrm{d}\theta}{\mathrm{d}t} = \frac{1}{N_{\mathrm{surf}}} \left(j_{\mathrm{ads}} - j_{\mathrm{des}} - N_{\mathrm{bulk}} D_{\mathrm{H}} \left. \frac{\partial C_{\mathrm{H}}}{\partial r} \right|_{R_0} \right) \tag{11}$$

$$\frac{\partial C_{\mathrm{H}}(r)}{\partial t} = \frac{\partial D_{\mathrm{H}}}{\partial r} \frac{\partial C_{\mathrm{H}}}{\partial r} + D_{\mathrm{H}} \left(\frac{\partial^2 C_{\mathrm{H}}}{\partial r^2} + \frac{2}{r} \frac{\partial C_{\mathrm{H}}}{\partial r} \right) + u_{\mathrm{dec}} \tag{12}$$

$$\frac{\partial C_{\mathrm{MH}}(r)}{\partial t} = -u_{\mathrm{dec}}, \tag{13}$$

where N_{bulk} is the site density in Mg. In eq 12, note the existence of the first term of the right-hand side due to the spatial variation of D_{H}. Incidentally, the time evolution of C_{MH} is analytically solved for eqs 10 and 13 as:

$$C_{\mathrm{MH}}(r,t)=\begin{cases}0 & \text{(in absorption process)}\\ C_{\mathrm{MH}}(r,0)\exp\left[-k_{\mathrm{dec}}^{0}\exp\left(-\dfrac{E_{\mathrm{dec}}}{RT}\right)t\right] & \text{(in desorption process)}\end{cases}. \qquad (14)$$

Because of the spherical symmetry, there assumed to be no flux of hydrogen at the core ($r = 0$) as:

$$j_{\mathrm{dif}}(0)=0. \qquad (15)$$

Considering hydrogen absorption into the Mg particles and hydrogen desorption from the MgH_2 particles, the initial conditions of concentration distribution are given by:

$$t=0:\theta=0,\ C_{\mathrm{H}}(r)=0,\ C_{\mathrm{MH}}(r)=0\ \ (0\le r<R_0) \qquad (16)$$

for the absorption process, and

$$t=0:\theta=1,\ C_{\mathrm{H}}(r)=0,\ C_{\mathrm{MH}}(r)=n\ \ (0\le r<R_0) \qquad (17)$$

for the desorption process. We solve the mass balance equations (eqs 11-13), under the conditions of eqs 3 and 15-17, using the finite-difference method to compute the time evolution of the hydrogen concentration profile.

3. RESULTS AND DISCUSSION

3.1. Reproduction of experimental results by the model

In this study, we adopted the experimental data of Huot *et al.*[14] for hydrogen absorption and desorption on Mg particles with a radius of 10 μm to evaluate the validity of our model and to determine the parameters. By varying s^0, E_{ads}, k^0_{des}, E_{des}, k^0_{dec}, and E_{dec}, we reproduced the experimental data for the absorption and desorption processes using our model, as shown in Figure 3. The determined parameters and the parameters we used are listed in Table 1. We incidentally set different E_{des} values for the absorption and desorption processes, assuming different hydrogen potentials in the metals for the two processes because the hydrogen absorption and desorption processes on metals show hysteresis. The determined E_{ads} and E_{des} for the desorption process are consistent with the data presented in Reference 25 (E_{ads} = 72 kJ mol^{-1}, E_{des} = 136 kJ mol^{-1}). On the other hand, E_{des} for the absorption process was calculated to be larger than that for the desorption process, presumably because of the ease of desorption due to the lattice-structure change by the hydrogen intake. It should be noted that for nanostructured metals the mechanical stress in the material induces significant effects on the kinetic as well as equilibrium properties for transportation on conditions, as experimentally and numerically reported.[34-36] Our present model is thus valid for metal particles with diameters larger than ~100 nm, and a proper formulation modification for the strain effect will be needed to apply for nanoscale particles.

3.2. Analysis of the absorption/desorption rates

The overall rate of absorption and desorption, v, is defined in eq 18. We compare the observed absorption and desorption rates, v_{obs}, with the virtual rates to clarify the rate-determining steps in the absorption and desorption processes by assuming that some elementary step(s) are rate-

determining. Namely, we compared v_{obs} with the virtual rates (v_{surf}, v_{dif}, $v_{dif\text{-}reac}$, and v_{reac}) when the surface adsorption/desorption, internal diffusion, internal diffusion/chemical reaction, and chemical reaction, respectively, are rate-determining.

$$v = \left| \frac{\mathrm{d}X}{\mathrm{d}t} \right| \tag{18}$$

Next, we investigate the regimes of the surface absorption and desorption control. For surface control, diffusion is sufficiently fast; therefore, the hydrogen concentration can be considered uniform in the Mg particle. We can calculate the time evolution of X using eq 19 under the condition of eq 20.

$$\frac{\mathrm{d}X}{\mathrm{d}t} = \frac{3}{R_0} \frac{N_{surf}}{N_{bulk}} \left(j_{ads} - j_{des} \right) \tag{19}$$

$$X = C(r) \ \left(0 \le r \le R_0 \right) \tag{20}$$

We investigate the diffusion-controlled absorption processes and the diffusion-and-reaction-controlled desorption processes. In these cases, hydrogen adsorption and desorption on the Mg surface are assumed to be in equilibrium; therefore, the surface coverage is given by eqs 21 and 22:

$$\theta = \theta_{eq} \tag{21}$$

$$2 s^0 \Gamma_{H_2} \exp\left(-\frac{E_{ads}}{RT} \right) \left(1 - \theta_{eq} \right)^2 - k_{dec}^0 \exp\left(-\frac{E_{des}}{RT} \right) N_{surf} {\theta_{eq}}^2 = 0 . \tag{22}$$

We can thus determine the time evolution of the hydrogen concentration using eqs 12 and 13 under the condition of eq 21. Lastly, we investigate the reaction-controlled desorption processes. For reaction-control, the hydrogen concentration is uniform in the Mg particle and the surface adsorption and desorption are always in equilibrium. We can therefore calculate the time evolution of the hydrogen concentration using eq 13 under the condition of eq 23:

$$\frac{\mathrm{d}C_{\mathrm{MH}}}{\mathrm{d}t} = -u_{\mathrm{dec}} \text{ and } C_{\mathrm{H}} = n\theta_{\mathrm{eq}}. \quad (23)$$

Figure 4 shows a comparison of observed hydrogen absorption rate, surface-controlled absorption rate, and diffusion-controlled absorption rates. For the absorption process, surface adsorption and desorption are rate-determining in the initial, low-loading regime because v_{obs} and v_{surf} are almost equal. For the experimental conditions of Huot *et al.*, shown in Figure 4a, the entire absorption process is likely surface-sorption controlled. However, as the Mg particle size or hydrogen partial pressure increases, as shown in Figures 4b-f, the influence of hydrogen diffusion in Mg becomes unignorable and diffusion becomes the rate-determining step in the high-loading regime after absorption proceeds (Figure 4f). The tendency that the system shifts toward diffusion-control as the particle size increases is simply attributed to the increased hydrogen diffusion distance. The tendency that the system shifts toward diffusion-control under a high hydrogen partial pressure is likely caused by a high hydrogen concentration region formed around the particle surface that hinders hydrogen diffusion—the high pressure increases the hydrogen flux toward the surface. This phenomenon is called the *shell effect*, and it is consistent with experimental reports[10,11].

Figure 5 shows results that compare observed hydrogen desorption rate, surface-controlled desorption rate, diffusion and reaction-controlled desorption rates, and reaction-controlled desorption rates for various particle sizes. The system is assumed to be almost reaction-controlled as the particle radius decreases to approximately 1 μm (Figure 5a) while shifting toward surface-sorption-control as the particle size increases (Figure 5c). In Figure 5b, transportation in the system is dominated by hydrogen diffusion in the hydride region in the initial, high-loading regime. The

desorption rate is extremely slow, but a rate-determining-process transition is seen, in which the desorption rate approaches the rate for the surface-control condition as desorption proceeds.

3.3. Effects of transition-metal doping

As a case study to utilize our model for designing improved Mg-based hydrogen-storage systems, we investigate the effect of adding a catalyst to Mg. Many reports have examined the enhancement of hydrogen dissociation and recombination on a Mg surface by doping transition metals in the Mg surface. Pozzo *et al.*[37], for example, showed the large effectiveness of Ni doping, and calculated an activation energy of 5.76 kJ mol^{-1} for hydrogen dissociation on a Ni-doped Mg surface. From this result, we calculate a decrease in the activation energy (ΔE) for hydrogen dissociation and recombination on the Mg adsorption sites of 66.24 kJ mol^{-1}. We then assume that E_{ads} and E_{des} both decrease by ΔE because of Ni doping, as shown in Figure 2. We investigate the change in the absorption and desorption rates for Ni doping in Mg using our model. The surface adsorption and desorption flux for transition-metal doping to the Mg surface is described by eqs 24 and 25.

$$j_{\mathrm{ads}} = 2s^0\Gamma_{\mathrm{H_2}} \exp\left(-\frac{E_{\mathrm{ads}} - \Delta E}{RT}\right)(1-\theta)^2\phi + 2s^0\Gamma_{\mathrm{H_2}} \exp\left(-\frac{E_{\mathrm{ads}}}{RT}\right)(1-\theta)^2(1-\phi) \tag{24}$$

$$j_{\mathrm{des}} = k_{\mathrm{des}}^0 \exp\left(-\frac{E_{\mathrm{des}} - \Delta E}{RT}\right)N_{\mathrm{surf}}\theta^2\phi + k_{\mathrm{des}}^0 \exp\left(-\frac{E_{\mathrm{des}}}{RT}\right)N_{\mathrm{surf}}\theta^2(1-\phi), \tag{25}$$

where ϕ is the doping ratio, which is the molar fraction of the additive on the Mg surface.

Figure 6 shows our simulation result. The addition of a small amount of Ni significantly enhances the absorption rate, as shown in Figure 6a, and the absorption-rate changes by doping at 423 K. Most of the absorption process is limited by surface adsorption, which causes the enhancement. Sufficient rates are obtained by doping, even at temperatures as low as room temperature, because the equilibrium absorption amount is larger at lower temperatures. Figure 6b shows the changes in the desorption rate at 623 K and 648 K. The desorption rate also increases

after doping, but the change is not as dramatic as that for the absorption rate. This result likely occurs because surface sorption and the internal diffusion and reaction dominate the desorption process. Heating to approximately 600 K may be required, even though the desorption rate is slightly improved by doping, because higher temperatures are advantageous for desorption in equilibrium; therefore, another treatment may be needed to decrease the operational desorption temperature. It should be noted that while this case study is calculated for Ni doping, our model is applicable also for other effective transition-metal dopants such as Fe[38], Co[39], Nb[40], and Rh[37], simply by adopting corresponding activation energies[37] for hydrogen dissociation on the doped Mg surfaces.

4. CONCLUSION

A detailed model was constructed to account for multiple elementary steps in the kinetics of hydrogen absorption and desorption on Mg. Our model successfully reproduced a series of experimental data for both absorption and desorption processes. We clarified the transitions of the rate-determining steps in the absorption and desorption processes from surface sorption to diffusion and chemical reaction as the hydrogen concentration in Mg increased. We demonstrated that our model can quantitatively estimate the changes in the absorption and desorption rates based on changes in the operational conditions, such as the metal particle size, temperature, pressure, and surface doping of transition metals. Our model is thus likely to be a useful tool to provide design principles to improve the performance of metal hydrogen-storage systems.

AUTHOR INFORMATION

Corresponding Author

*Email: tanabe@cheme.kyoto-u.ac.jp

ACKNOWLEDGMENT

This work was partially supported by JFE 21st Century Foundation and Futaba Electronics Memorial Foundation.

REFERENCES

(1) Schlapbach, L.; Züttel, A. Hydrogen-Storage Materials for Mobile Applications. *Nature* **2001**, *414*, 353–358.

(2) Züttel, A. Materials for Hydrogen Storage. *Mater. Today* **2003**, *6*, 24–33.

(3) Lai, Q.; Paskevicius, M.; Sheppard, D. A.; Buckley, C. E.; Thornton, A. W.; Hill, M. R.; Gu, Q.; Mao, J.; Huang, Z.; Liu, H. K.; et al. Hydrogen Storage Materials for Mobile and Stationary Applications: Current State of the Art. *ChemSusChem* **2015**, *8*, 2789–2825.

(4) Aguey-Zinsou, K.-F.; Ares-Fernández, J.-R. Hydrogen in Magnesium: New Perspectives toward Functional Stores. *Energy Environ. Sci.* **2010**, *3*, 526–543.

(5) Pedersen, A. S.; Kjøller, J.; Larsen, B.; Vigeholm, B. Magnesium for Hydrogen Storage. *Int. J. Hydrogen Energy* **1983**, *8*, 205–211.

(6) Lide, D. R. (Ed.) *CRC Handbook of Chemistry and Physics*, 80th ed.; CRC Press: Boca Raton (FL), USA, 1999.

(7) Fernández, J. F.; Sánchez, C. R. Rate Determining Step in the Absorption and Desorption of Hydrogen by Magnesium. *J. Alloys Compd.* **2002**, *340*, 189–198.

(8) Vegge, T. Locating the Rate-Limiting Step for the Interaction of Hydrogen with Mg(0001) Using Density-Functional Theory Calculations and Rate Theory. *Phys. Rev. B* **2004**, *70*, 035412.

(9) Nobuhara, K.; Kasai, H.; Diño, W. A.; Nakanishi, H. H_2 Dissociative Adsorption on Mg, Ti, Ni, Pd and La Surfaces. *Surf. Sci.* **2004**, *566–568*, 703–707.

(10) Luz, Z.; Genossar, J.; Rudman, P. S. Identification of the Diffusing Atom in MgH_2. *J. Less-Common Met.* **1980**, *73*, 113–118.

(11) Schlapbach, L. (Ed.) *Hydrogen in Intermetallic Compounds II*; Springer: Berlin, Germany, 1992.

(12) Jain, I. P.; Lal, C.; Jain, A. Hydrogen Storage in Mg: A Most Promising Material. *Int. J. Hydrogen Energy* **2010**, *35*, 5133–5144.

(13) Shim, J.-H.; Park, M.; Lee, Y. H.; Kim, S.; Im, Y. H.; Suh, J.-Y.; Cho, Y. W. Effective Thermal Conductivity of MgH_2 Compacts Containing Expanded Natural Graphite under a Hydrogen Atmosphere. *Int. J. Hydrogen Energy* **2014**, *39*, 349–355.

(14) Huot, J.; Liang, G.; Boily, S.; Van Neste, A.; Schulz, R. Structural Study and Hydrogen Sorption Kinetics of Ball-Milled Magnesium Hydride. *J. Alloys Compd.* **1999**, *293–295*, 495–500.

(15) Williams, M.; Sibanyoni, J. M.; Lototskyy, M.; Pollet, B. G. Hydrogen Absorption Study of High-Energy Reactive Ball Milled Mg Composites with Palladium Additives. *J. Alloys Compd.* **2013**, *580*, S144–S148.

(16) Hanada, N.; Ichikawa, T.; Fujii, H. Catalytic Effect of Nanoparticle 3d-Transition Metals on Hydrogen Storage Properties in Magnesium Hydride MgH_2 Prepared by Mechanical Milling. *J. Phys. Chem. B* **2005**, *109*, 7188–7194.

(17) Daryani, M.; Simchi, A.; Sadati, M.; Mdaah Hosseini, H.; Targholizadeh, H; Khakbiz, M. Effects of Ti-Based Catalysts on Hydrogen Desorption Kinetics of Nanostructured Magnesium Hydride. *Int. J. Hydrogen Energy* **2014**, *39*, 21007–21014.

(18) Jeon, K.; Moon, H. R.; Ruminski, A. M.; Jiang, B.; Kisielowski, C.; Bardhan, R.; Urban, J. J. Air-Stable Magnesium Nanocomposites Provide Rapid and High-Capacity Hydrogen Storage without Using Heavy-Metal Catalysts. *Nat. Mater.* **2011**, *10*, 286–290.

(19) Asano, K.; Westerwaal, R. J.; Anastasopol, A.; Mooij, L. P. A.; Boelsma, C.; Ngene, P.; Schreuders, H.; Eijt, S. W. H.; Dam, B. Destabilization of Mg Hydride by Self-Organized Nanoclusters in the Immiscible Mg-Ti System. *J. Phys. Chem. C* **2015**, *119*, 12157–12164.

(20) Asano, K.; Westerwaal, R. J.; Schreuders, H.; Dam, B. Enhancement of Destabilization and Reactivity of Mg Hydride Embedded in Immiscible Ti Matrix by Addition of Cr: Pd-Free Destabilized Mg Hydride. *J. Phys. Chem. C* **2017**, *121*, 12631–12635.

(21) Varin, R. A.; Czujko, T.; Chiu, C.; Wronski, Z. Particle Size Effects on the Desorption Properties of Nanostructured Magnesium Dihydride (MgH_2) Synthesized by Controlled Reactive Mechanical Milling (CRMM). *J. Alloys Compd.* **2006**, *424*, 356–364.

(22) Norberg, N. S.; Arthur, T. S.; Fredrick, S. J.; Prieto, A. L. Size-Dependent Hydrogen Storage Properties of Mg Nanocrystals Prepared from Solution. *J. Am. Chem. Soc.* **2011**, *133*, 10679–10681.

(23) Jia, Y.; Sun, C.; Shen, S.; Zou, J.; Mao, S. S.; Yao, X. Combination of Nanosizing and Interfacial Effect: Future Perspective for Designing Mg-Based Nanomaterials for hydrogen storage. *Renewable Sustainable Energy Rev.* **2015**, *44*, 289–303.

(24) Wang, Y.; Wang, Y. Recent Advances in Additive-Enhanced Magnesium Hydride for Hydrogen Storage. *Prog. Nat. Sci. Mater. Int.* **2017**, *27*, 41–49.

(25) Johansson, M.; Ostenfeld, C. W.; Chorkendorff, I. Adsorption of Hydrogen on Clean and Modified Magnesium Films. *Phys. Rev. B* **2006**, *74*, 193408.

(26) Seb Han, J.; Lee, J. Y. A Study of the Hydriding Kinetics of Mg_2Ni. *J. Less-Common Met.* **1987**, *131*, 109–116.

(27) Perejón, A.; Sánchez-Jiménez, P. E.; Criado, J. M.; Pérez-Maqueda, L. A. Magnesium Hydride for Energy Storage Applications: The Kinetics of Dehydrogenation under Different Working Conditions. *J. Alloys Compd.* **2016**, *681*, 571–579.

(28) Chou, K.-C.; Li, Q.; Lin, Q.; Jiang, L.-J.; Xu, K.-D. Kinetics of Absorption and Desorption of Hydrogen in Alloy Powder. *Int. J. Hydrogen Energy* **2005**, *30*, 301–309.

(29) Chou, K.-C.; Xu, K. A New Model for Hydriding and Dehydriding Reactions in Intermetallics. *Intermetallics* **2007**, *15*, 767–777.

(30) Evard, E.; Gabis, I.; Yartys, V. A. Kinetics of Hydrogen Evolution from MgH_2: Experimental Studies, Mechanism and Modelling. *Int. J. Hydrogen Energy* **2010**, *35*, 9060–9069.

(31) Fukai, Y.; Tanaka, K.; Uchida, H. *Suiso to kinzoku*; Uchida-roukakuho: Tokyo, Japan, 2002.

(32) Nishimura, C.; Komaki, M.; Amano, M. Hydrogen Permeation through Magnesium. *J. Alloys Compd.* **1999**, *293–295*, 329–333.

(33) Stioui, M.; Grayevsky, A.; Resnik, A.; Shaltiel, D.; Kaplan, N. Macroscopic and Microscopic Kinetics of Hydrogen in Magnesium-Rich Compounds. *J. Less-Common Met.* **1986**, *123*, 9–24.

(34) Baldi, A.; Narayan, T. C.; Koh, A. L.; Dionne, J. A. In Situ Detection of Hydrogen-Induced Phase Transitions in Individual Palladium Nanocrystals. *Nat. Mater.* **2014**, *13*, 1143–1148.

(35) Bannenberg, L. J.; Schreuders, H.; van Eijck, L.; Heringa, J. R.; Steinke, N.; Dalgliesh, R.; Dam, B.; Mulder, F. M.; van Well, A. A. Impact of Nanostructuring on the Phase Behavior of Insertion Materials: The Hydrogenation Kinetics of a Magnesium Thin Film. *J. Phys. Chem. C* **2016**, *120*, 10185–10191.

(36) Matsuda, A.; Mori, H. Theoretical Study on Crystal-Facet Dependency of Hydrogen Storage Rate for Shape Controlled Pd Nano Particles. *Chem. Phys. Lett.* **2016**, *644*, 255–260.

(37) Pozzo, M.; Alfè, D. Hydrogen Dissociation and Diffusion on Transition Metal (= Ti, Zr, V, Fe, Ru, Co, Rh, Ni, Pd, Cu, Ag)-Doped Mg(0001) Surfaces. *Int. J. Hydrogen Energy* **2009**, *34*, 1922–1930.

(38) Montone, A.; Aurora, A.; Gattia, D. M.; Antisari, M. V. Effect of Hydrogen Pressure and Temperature on the Reaction Kinetics between Fe-Doped Mg and Hydrogen Gas, *J. Alloys Compd.* **2011**, *509*, S580–S583.

(39) Jia, Y.; Cheng, L. N.; Pan, N.; Zou, J.; Lu, G. Q.; Yao, X. D. Catalytic De/Hydrogenation in Mg by Co-Doped Ni and VO_x on Active Carbon: Extremely Fast Kinetics at Low Temperatures and High Hydrogen Capacity, *Adv. Energy Mater.* **2011**, *1*, 387–393.

(40) Chen, M.; Cai, Z. Z.; Yang, X. B.; Zhu, M.; Zhao, Y. J. Theoretical Study of Hydrogen Dissociation and Diffusion on Nb and Ni Co-Doped Mg(0001): A Synergistic Effect, *Surf. Sci.* **2012**, *606*, L45–L49.

Table 1. Model parameters for the simulation

Parameter	Value	Units	Reference
s^0	0.0024	-	This work
k^0_{des}	1.2×10^{13}	s^{-1}	This work
k^0_{dec}	1.69×10^{14}	-	This work
D^0_H	1.54×10^{-6}	$m^2\ s^{-1}$	Nishimura, 1999[32]
E_{ads}	72	kJ mol^{-1}	This work
E_{des}	170[a], 136[b]	kJ mol^{-1}	This work
E_{dif}	24.1	kJ mol^{-1}	Nishimura, 1999[32]
E_{dec}	205	kJ mol^{-1}	This work
β	16.6	-	This work
N_{surf}	3.22×10^{-5}	mol m^{-2}	Johansson, 2006[25]
N_{bulk}	7.15×10^{4}	mol m^{-3}	This work

[a]Parameter for the absorption process. [b]Parameter for the desorption process.

Figure Captions

Figure 1. Conceptual schematic of our hydrogen-dynamic model. j_{ads}, j_{des}, and j_{dif} denote the fluxes of hydrogen dissociative adsorption, recombinative desorption, and diffusion, respectively.

Figure 2. Potential energy diagram of hydrogen in the gas phase and in Mg. E_{ads}, E_{des}, and E_{dif} denote the activation energies of surface adsorption, desorption, and diffusion, respectively. ΔE denotes suppression of the activation energy of surface adsorption and desorption by addition of a catalyst.

Figure 3. (a) Hydrogen absorption curves for Mg particles under a hydrogen pressure of 1.0 MPa. (b) Hydrogen desorption curves for MgH_2 particles under a hydrogen pressure of 0.015 MPa. (marks: experimental data, lines: calculation result).

Figure 4. Calculated observed hydrogen absorption rate, v_{obs} (dark blue lines), surface-controlled absorption rate, v_{surf} (red lines), and diffusion-controlled absorption rates, v_{dif} (green lines). Red shaded regions indicate the surface-controlled regimes, and green shaded regions indicate diffusion-controlled regimes. In this simulation, $T = 673$ K.

Figure 5. Calculated observed hydrogen desorption rate, v_{obs} (dark blue lines), surface-controlled desorption rate, v_{surf} (red lines), diffusion and reaction-controlled desorption rates, $v_{dif\text{-}reac}$ (green lines), and reaction-controlled desorption rates, v_{reac} (light blue lines). Red shaded regions indicate surface-controlled regimes, and blue shaded regions indicate reaction-controlled regimes. In this simulation, $T = 648$ K and $P_{H_2} = 0.015$ MPa.

Figure 6. Effect of doping ratio of Ni on kinetics of hydrogen (a) absorption and (b) desorption for Mg particles.

Figures

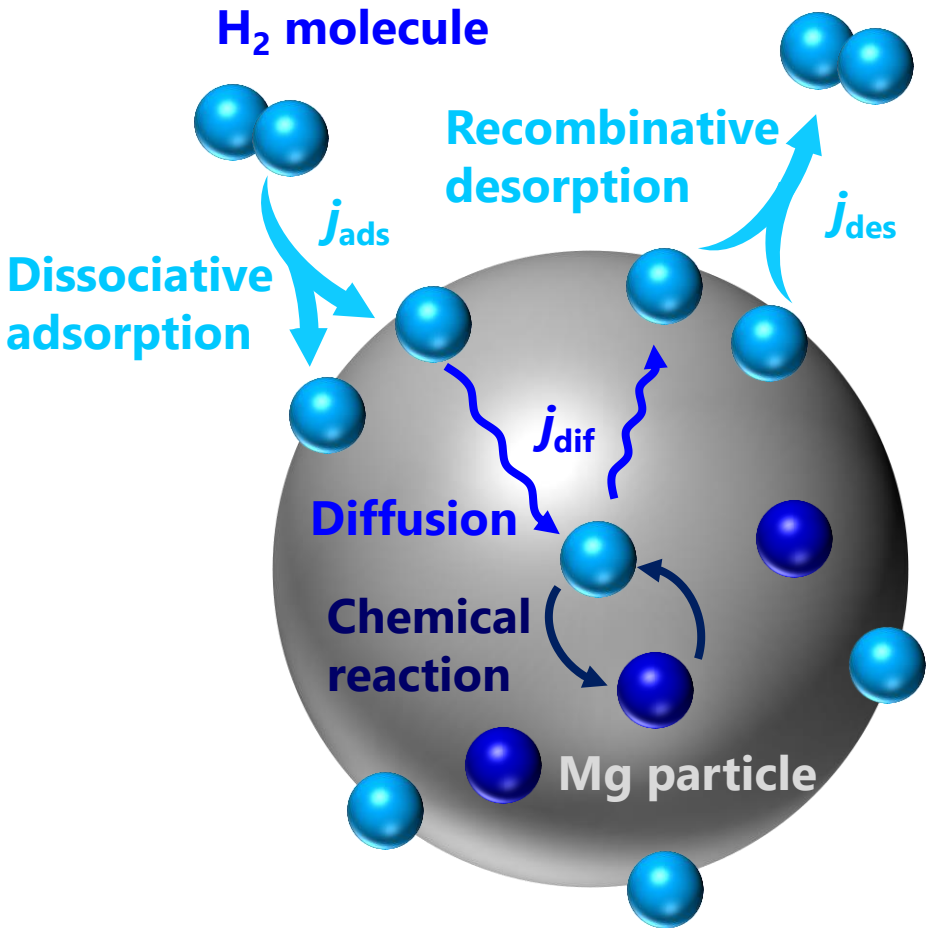

Figure 1

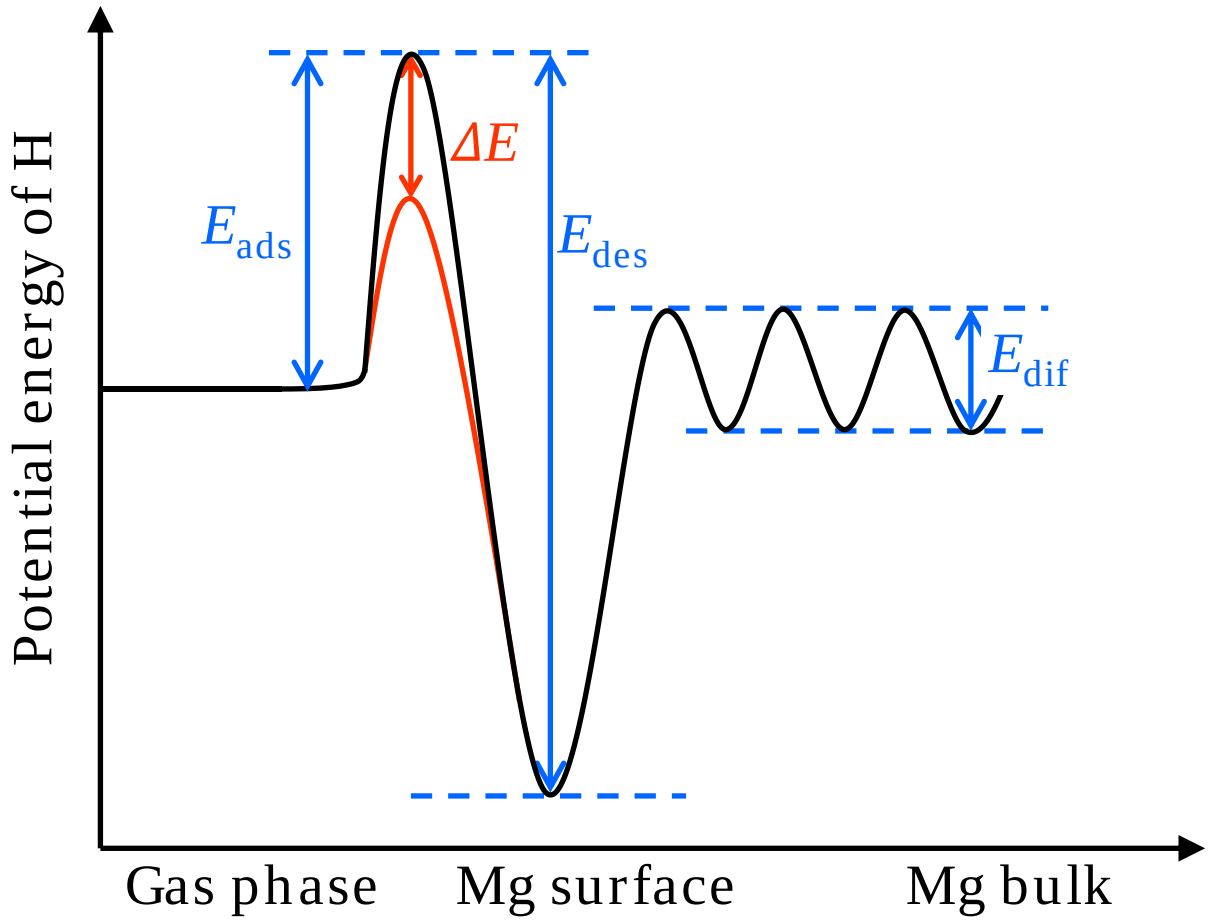
Potential energy of H
E_{ads}
ΔE
E_{des}
E_{dif}
Gas phase
Mg surface
Mg bulk

Figure 2

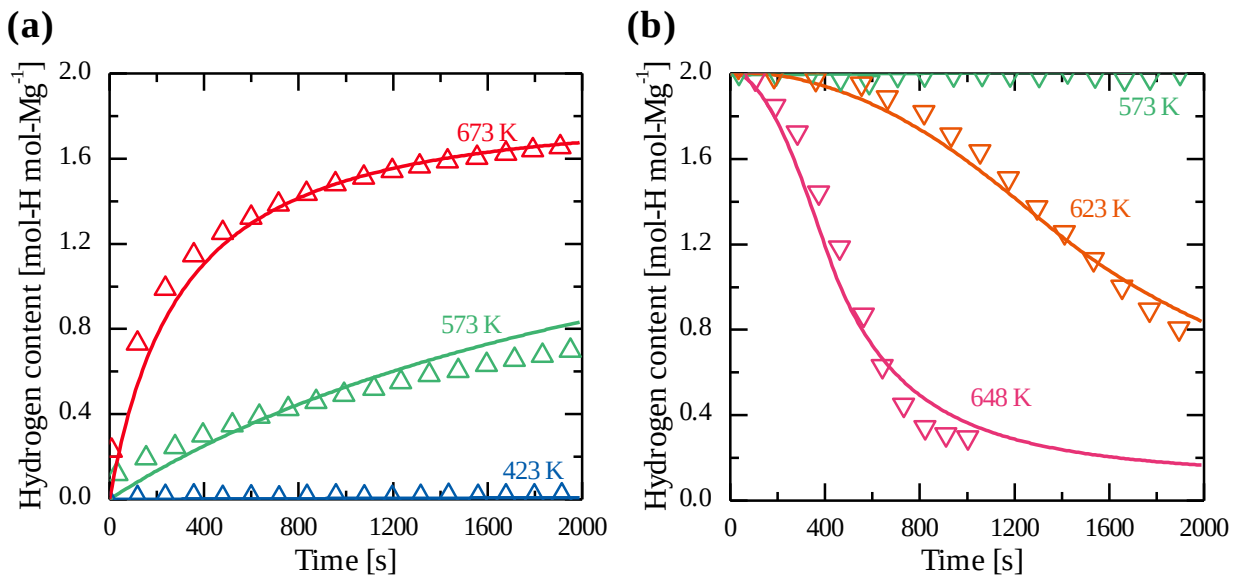
(a)
(b)
Hydrogen content [mol-H mol-Mg-1]
Time [s]
673 K
573 K
423 K
623 K
648 K
0.0
0.4
0.8
1.2
1.6
2.0
0
400
800
1200
1600
2000

Figure 3

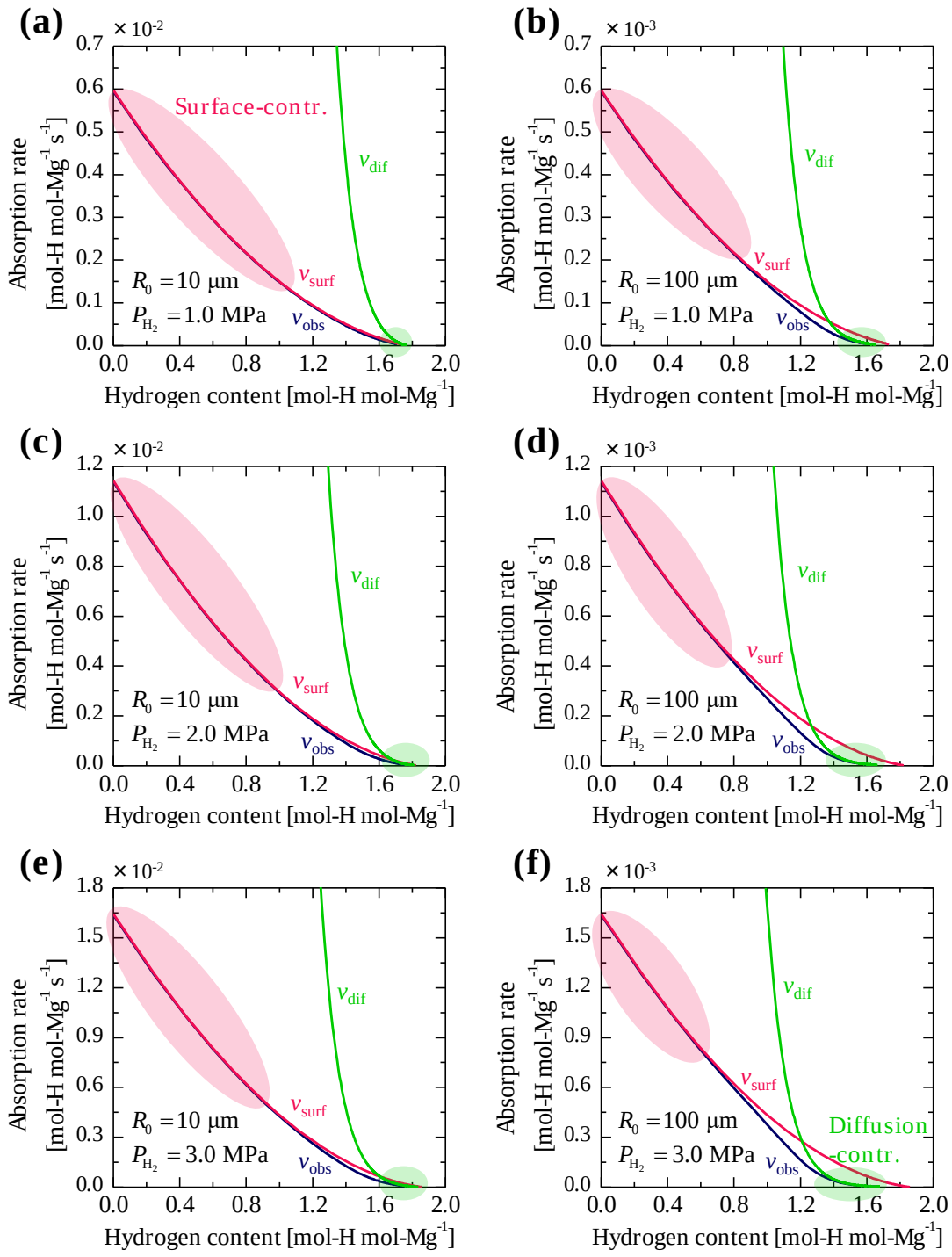
(a)
× 10-2
Surface-contr.
v_{dif}
v_{surf}
v_{obs}
R_0 = 10 μm
P_{H_2} = 1.0 MPa
Absorption rate [mol-H mol-Mg-1 s-1]
Hydrogen content [mol-H mol-Mg-1]
(b)
× 10-3
R_0 = 100 μm
P_{H_2} = 1.0 MPa
(c)
× 10-2
R_0 = 10 μm
P_{H_2} = 2.0 MPa
(d)
× 10-3
R_0 = 100 μm
P_{H_2} = 2.0 MPa
(e)
× 10-2
R_0 = 10 μm
P_{H_2} = 3.0 MPa
(f)
× 10-3
R_0 = 100 μm
P_{H_2} = 3.0 MPa
Diffusion -contr.

Figure 4

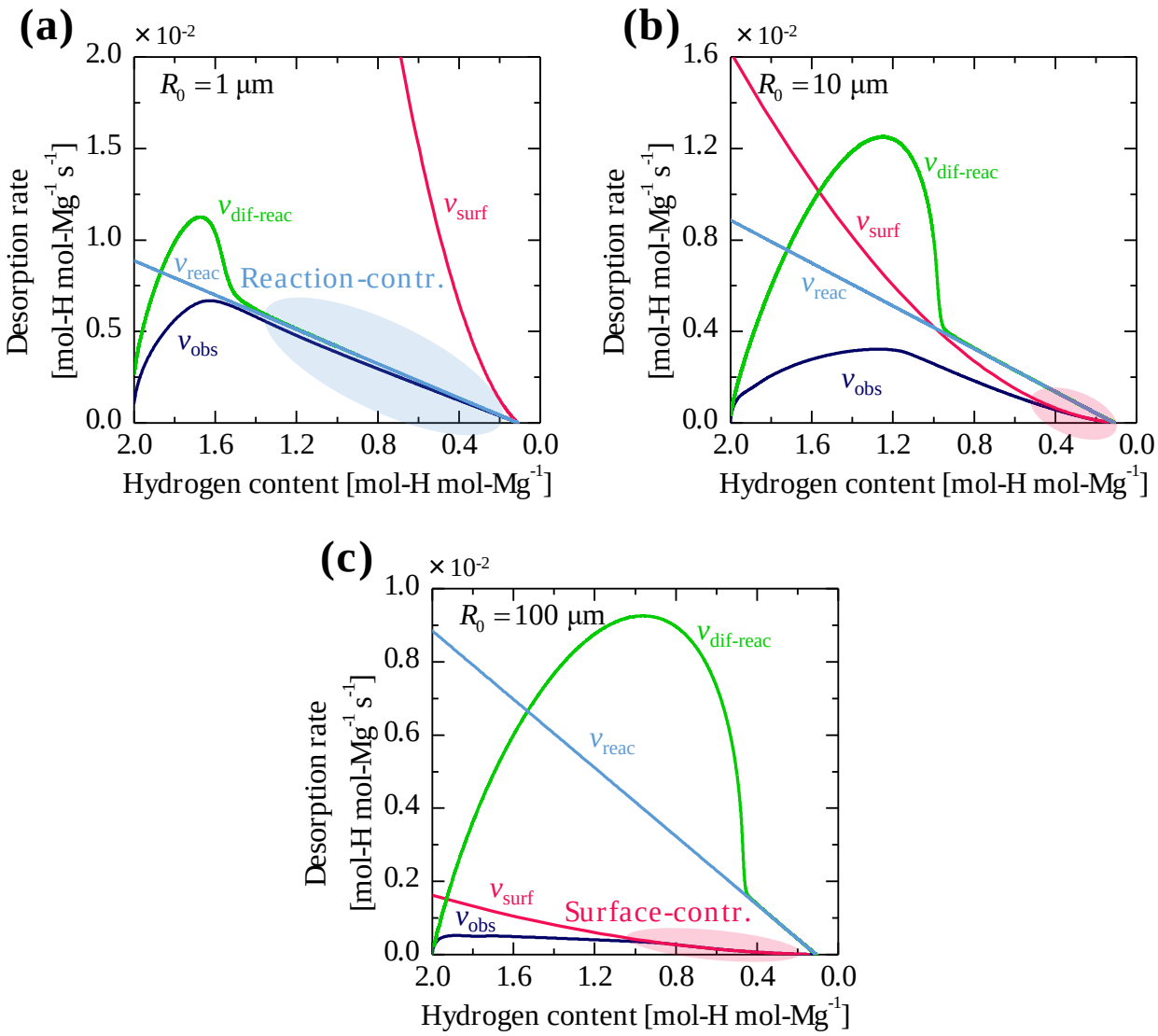
(a)
× 10-2
R0 = 1 μm
vdif-reac
vsurf
vreac
Reaction-contr.
vobs
Desorption rate [mol-H mol-Mg-1 s-1]
Hydrogen content [mol-H mol-Mg-1]
(b)
× 10-2
R0 = 10 μm
vdif-reac
vsurf
vreac
vobs
Desorption rate [mol-H mol-Mg-1 s-1]
Hydrogen content [mol-H mol-Mg-1]
(c)
× 10-2
R0 = 100 μm
vdif-reac
vreac
vsurf
Surface-contr.
vobs
Desorption rate [mol-H mol-Mg-1 s-1]
Hydrogen content [mol-H mol-Mg-1]

Figure 5

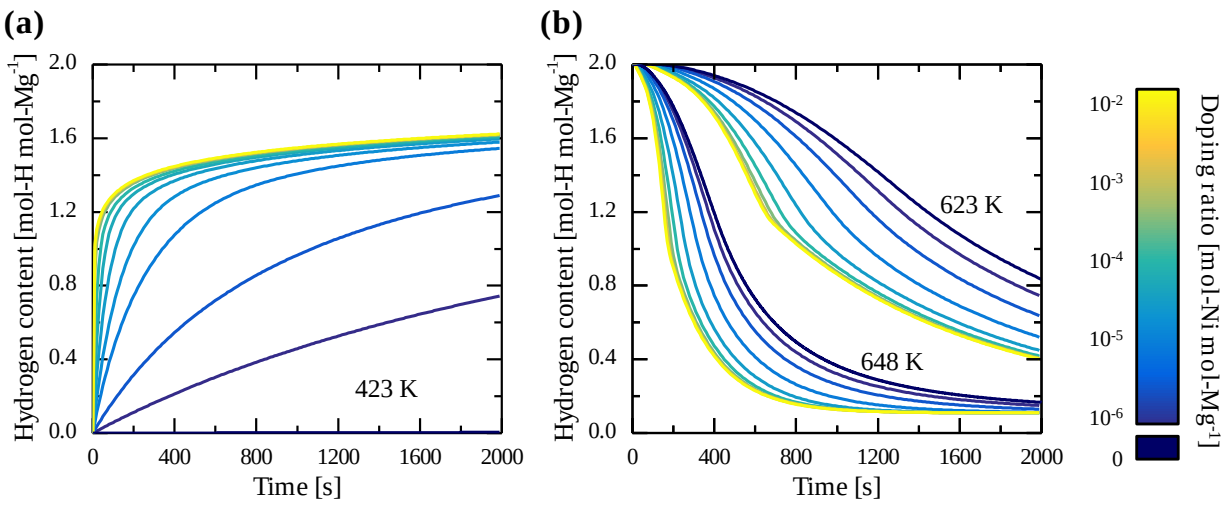
(a)
(b)
Hydrogen content [mol-H mol-Mg-1]
Time [s]
423 K
623 K
648 K
Doping ratio [mol-Ni mol-Mg-1]

Figure 6